Single CdSe/ZnS Nanocrystals in an Ion Trap: Charge and Mass Determination and Photophysics Evolution with Changing Mass, Charge, and Temperature

David M. Bell, Collin R. Howder, Ryan C. Johnson, and Scott L. Anderson*

Department of Chemistry, University of Utah, Salt Lake City, Utah 84112, United States

ABSTRACT We report measurements of fluorescence intermittency (blinking) and spectral behavior for single semiconductor nanocrystal quantum dots (QDs) isolated in the gas phase and discuss the effects on fluorescence of the QD charge state and heating to the point of sublimation. Core—shell CdSe/ZnS QDs were trapped in a quadrupole ion trap and detected by laser-induced fluorescence. The mass (*M*) and charge (*Q*) were determined nondestructively, and both were followed continuously over the course of hours or days. Emission spectra of the trapped QDs are significantly red-shifted relative to the solution-phase emission from the same particles. The temperature of the trapped QDs is determined by the balance between laser heating and collisional cooling and thermal emission, and it is possible to heat the particles to remove ligands or to the point of sublimation. QDs are observed to be emissive during sublimation, for up to 85% mass loss, with emission intensity roughly proportional to the surface area. Eventually, the fluorescence quantum yield drops suddenly, and the QDs begin to blink. The method used is versatile and will allow studies of quantum dot optical properties as a function of size, ligand removal, heating, surface oxidation, and other manipulations, where these properties are continuously correlated with the mass and charge.

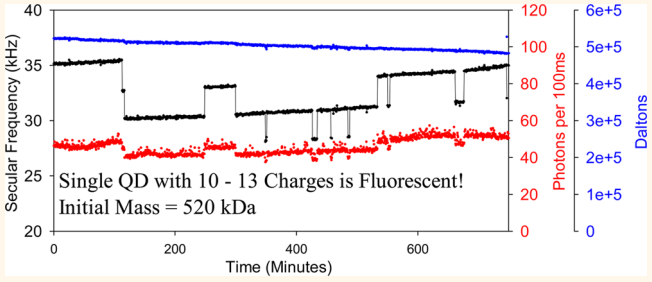

KEYWORDS: quantum dots · ion trap · single particle · blinking · mass spectrometry

Nanoparticle mass spectrometry (NPMS) and opto-mechanical levitation provides an interesting and useful way to study the physical and optical properties of levitated nanostructures.[1−8] NPMS allows for repeated, nondestructive measurements of the mass, *M*, and charge, *Q*, of single trapped nanoparticles, making it possible to study correlations between *M*, *Q*, surface chemistry, and optical properties, as particles are manipulated by heating, exposed to reactants, *etc.*[1,4,9−15] As discussed below, the mass and charge are obtained by observing the particle's motion in a quadrupole trap, using either light scattering or fluorescence to track the motion. In addition to obtaining *M* and *Q*, it is possible to measure optical properties, such as the emission spectrum, temporal behavior such as blinking (intermittent fluorescence) or bleaching, and to correlate the appearance of these optical effects with changes in particle mass, charge, or surface chemical state. Here we report blinking and spectral behavior for single charged semiconductor nanocrystal quantum dots (QDs) isolated in the gas phase and discuss the effects on fluorescence of charge state, heating, and mass loss by sublimation.

The basis of the NPMS method is to trap a single, charged nanoparticle in a quadrupole ion trap, using light scattering or laser-induced fluorescence (LIF) to detect and track the motion of the particle. The motional secular frequency (ω_z) of a charged particle in such a trap is inversely proportional to the mass/charge ratio, M/Q.[16] By making repeated measurements over the course of hours or days, it is possible track the emission properties and to observe how

* Address correspondence to anderson@chem.utah.edu.

Received for review November 14, 2013 and accepted January 10, 2014.

Published online January 10, 2014
10.1021/nn405920k

they respond to changes in M/Q as the particle is heated, exposed to reactants, or otherwise manipulated. By allowing occasional collisions with ions, electrons, or metastables created in a discharge, the charge, Q, can be changed. By measuring the change in secular frequency accompanying Q changing by one elementary charge ($\Delta\omega_z/e$), the exact value of Q is determined.[1,9,11] With Q, we obtain M, limited only by the precision of the ω_z measurement, which can be as high as 1 ppm.[9]

CdSe nanocrystals, also known as quantum dots, are too small to efficiently scatter light but are efficient emitters (quantum yield 50−85%)[17,18] with interesting photophysics, making them good candidates for NPMS. For NPMS, the QDs must be charged, so one important issue is the effect of charging on fluorescence intensity. A number of groups have examined the effects of charging QDs on various electrodes or in solution.[19−26] Guyot-Sionnest and co-workers attached QDs to an electrode and quenched fluorescence by applying a negative voltage (−1 V) to the electrode. This quenching was reversible by applying a slight positive charge (+0.3 V).[22] Galland *et al.* recently used a similar approach to gather fluorescence information while simultaneously collecting lifetimes.[24] In this study, there were two types of blinking behavior with distinct lifetimes and blinking on/off statistics that could be controlled electrochemically. One type was due to Auger recombination and another due to interactions between the Fermi level of the electrode and the trap states present on the QDs. Interestingly, a QD could exhibit both types of blinking mechanisms at different times, meaning that blinking is not due to the chemical makeup of an individual QD, but rather is inherent to QDs.[24]

QDs have been studied extensively in solution[27−29] or on surfaces,[22,30−32] but little is known about their optical properties when they are charged and detached from a surface.[33] In summary, it is not obvious what might be expected for fluorescence of QDs in the gas phase with up to 20 charges, in the form of Na^+ adsorbed on the surface. In this paper, we present observations of fluorescence from single QDs isolated in the gas phase in a quadrupole ion trap, shown in Figure 1, and demonstrate determination of the absolute mass and charge for both individual QDs and small QD aggregates. In addition, we examine emission intensities and spectral properties over time as the QDs are heated to the point of sublimation and undergo charge changes.

RESULTS

Measuring *M/Q via* Secular Frequency Measurement. As discussed below in the Methods section, the mass-to-charge ratio (M/Q) is determined by measuring the secular frequency for motion of the QD in the trap, and

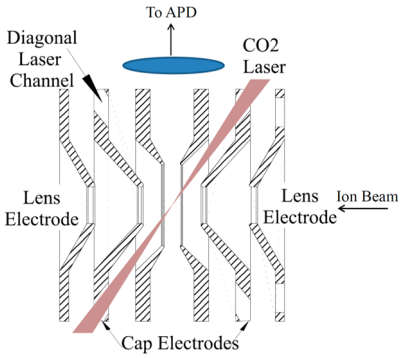

Figure 1. Cross sectional view of the trap along the *x*-axis. Light is collected on the vertical axis, and the 532 nm laser is introduced into the plane of the image in the center of the trap. Diagonal channels are used to introduce the CO_2 laser. The horizontal axis is used to introduce the ions to the trap.

the approach we have found best for secular frequency measurement is to apply a sinusoidal "drive" signal to one of the lens electrodes, shown in Figure 1, just outside the trap, creating a sinusoidal field that penetrates to the trap center. The field is too weak to have significant effect on the trapped QD motion, except when the drive frequency is resonant with the QD axial secular frequency, ω_z. On resonance, the amplitude of the ω_z oscillations becomes large enough to reduce the fraction of time that the QD spends in the detection volume, resulting in a drop in LIF signal. The detection volume is determined by the overlap of the LIF laser focus and APD imaging lens focus and has characteristic dimensions of roughly 50−100 μm. It is possible to obtain parts per million mass precision in slow scans with low drive amplitudes and low pressure,[9] but here the goal was to follow changes in QD properties over time; therefore, the sweeps were fast (>1 kHz/s), and a high (2 V) drive amplitude was used to ensure measurable response during the short time on resonance. To measure the fast sweeps, short dwell times were also needed, resulting in poor signal/noise. Figure 2 shows an example of a single sweep (data points) as well as the average of five sweeps scanned both to higher (20−60 kHz) and to lower (60−20 kHz) frequency. Note that the sweeps to higher and lower frequencies both show a sharp resonance at 32.67 kHz, and even in the single scan, the signal dip is well outside the scatter in the data points. The ω_z resonance appears as a peak in these data because the experiments were done with the trap filled to 1 mTorr with argon (P_{trap} = 1 mTorr). As a result, the driven motion excited at resonance is quickly damped by Ar collisions, resulting in quick signal recovery as the drive voltage scan away from resonance. This damping also, in principle, broadens the resonance, degrading precision; however, in this case, the factor limiting precision is the scan rate. By performing repeated frequency sweeps, the secular frequency (*i.e.*, M/Q) for a single QD can be tracked for many hours. To extract the ω_z values for each sweep,

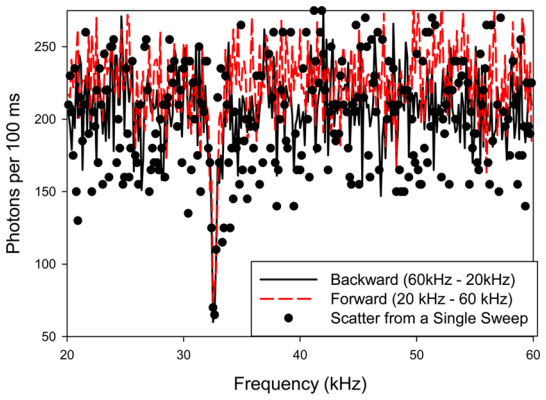

Figure 2. Sweeps across the secular frequency resonance for a single particle in the trap. The solid black line corresponds to an average of 5 sweeps from 60 to 20 kHz. The dashed red line corresponds to an average of 5 sweeps from 20 to 60 kHz. The scatter plot shows a noise in a single sweep.

the negative peak, as seen in Figure 2, is fit with a Gaussian, the center of which is reported as ω_z.

Note that the scatter in the single scan data points is substantially greater than would be expected for statistical noise. The scatter partly reflects fluctuations in particle position due to thermal (Brownian) motion of the QD. Decker has discussed the expected amplitude of thermal motion, which scales like $(TM/Q^2)^{1/2}$, and for QDs with T = 300 K, the root mean square excursions are on the order of 30 and 60 μm, respectively, in the axial and radial directions.[34] These are comparable to the dimensions of our detection volume, thus thermal motion leads to real fluctuations in LIF intensity.

The fact that a single peak is observed in the frequency spectrum indicates that there is only one particle in the trap. When more than one particle is trapped, multiple peaks are observed because the charge on these small QDs is low enough that coupling between the particles is weak compared to thermal energy; that is, each particle behaves quasi-independently with its own ω_z resonance. In principle, it is possible that a single peak could result from two or more particles which coincidently happen to have nearly identical ω_z values; however, this unlikely situation would be revealed as soon as one of the particles changed charge.

Tracking *M/Q* and Determination of *Q* and *M*. Figure 3 shows an example time record for a single QD observed for 12.5 h at low enough LIF laser intensity (100 W/cm^2) to minimize mass or other changes due to heating. The secular frequency (ω_z) shows discrete steps corresponding to events where QD charge changed by one elementary unit ($\Delta Q = \pm e$). Charge changes occur due to occasional (~1/h) collisions of the QD with electrons, ions, or metastables in the chamber background, and because we need such events to determine Q and M,[11] a cold cathode gauge is left on to create electrons, Ar^+, and Ar* from the 1 mTorr argon buffer gas. In this case, $\Delta\omega_z/e = 2682 \pm 44$ Hz, as determined by fitting the 16 steps observed. From $\omega_z/\Delta\omega_z$, we can determine Q at each step (values indicated on the figure), and once we know Q, we can convert M/Q to M, which is also plotted on the figure. In this case, the mass record is deliberately boring—just a gradual loss (0.5% per hour) of mass, due to mild heating from the LIF laser.

The diameter of these (NN-labs) QDs is reported to be 6 ± 0.6 nm, which corresponds to roughly a factor of 2 variation in mass, with estimated masses ranging from ~480 kDa to ~1.1 MDa, not including the ligand layer. (The masses are estimated assuming a nominal ZnS shell thickness of 1 nm and using bulk densities for CdSe and ZnS. For the nominal 6 nm QD, the core and shell masses are nearly equal.) For core−shell CdSe/ZnS, it has been shown that between 800 and 1000 dithiocarbamate ligands are present.[35] If we presume the same coverage (~18 Å^2/molecule) on a 6 nm QD, there should be ~630 ligands present with a mass of ~137 kDa for the nascent QD. However, we believe that there is significant ligand desorption/decomposition because the freshly trapped QDs are briefly heated using a CO_2 laser as described below. In this example, the mass is near the low end of the expected mass range, and therefore, we can safely conclude that the particle was a single QD, presumably having lost most of the ligand mass.

Figure 3 also shows the LIF intensity as a function of time, and it can be seen that there are steps in LIF intensity that track the charge steps in ω_z. These do not represent real changes in the fluorescence quantum yield with charge. Instead, they result from the effects of charge on photon collection efficiency. Recall that the root mean square amplitude of thermal motion of the QD scales like $(TM/Q^2)^{1/2}$, and that the amplitudes are comparable to the detection volume defined by the laser and APD foci. Therefore, when Q increases (decreases) by e, the rms thermal amplitude decreases (increases) by 8−10%, resulting in a small increase (decrease) in collection efficiency. The detection volume can be increased to avoid this effect, but that decreases the sensitivity for measuring ω_z, requiring higher drive amplitudes. In the figures below, small fluctuations in LIF, correlated with charge steps, should be ignored.

Effects of Heating and Particle Sublimation. Figure 4 shows the first ~83 h of the time record for a single particle tracked for more than 4 days, during which time we substantially changed the particle properties by driving large mass losses. Emission spectra were acquired during several intervals, by swapping filters on the APD, turning the laser intensity back to the initial low level for each spectral measurement. These intervals of low laser intensity are delineated by pairs of vertical lines. To allow the changes in particle properties to be seen more clearly, Figure 5 shows the data

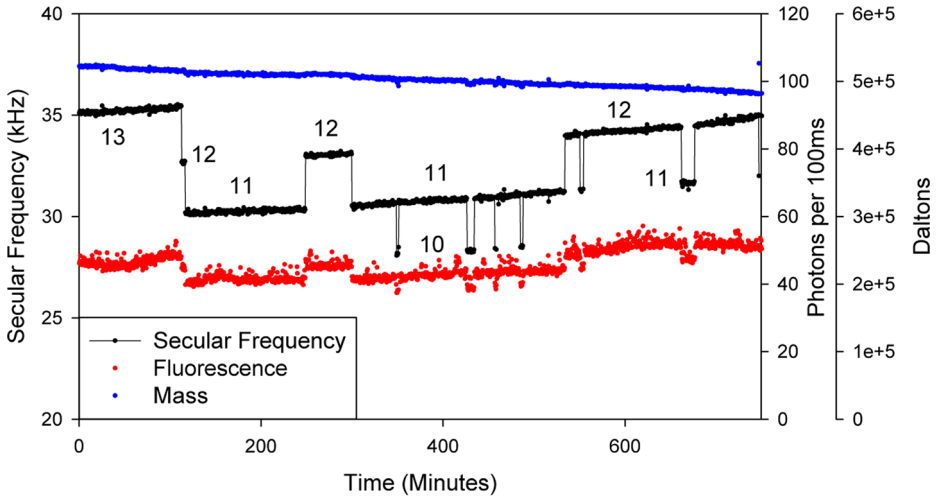

Figure 3. Time record (12.5 h) for a single trapped quantum dot, showing variations in secular frequency (kHz, black), mass (Da, blue), and fluorescence intensity (photons per 100 ms, red). The number of charges present is shown.

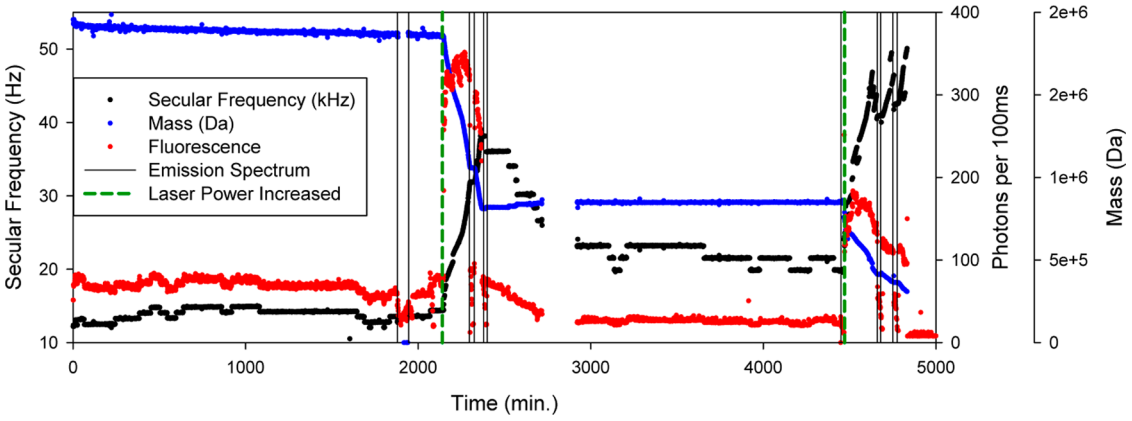

Figure 4. Time record of secular frequency (kHz, black), mass (Da, blue), and fluorescence intensity (photons per 100 ms, red) for a single small quantum dot aggregate, observed for 4 days. Pairs of vertical black lines indicate intervals when emission spectra were taken. The laser power density was 100 W/cm^2 except between 2100 and 2370 min and 4470 and 5000 min when it was increased to 216 W/cm^2 to increase the particle temperature. The laser power density was turned down to 100 W/cm^2 when emission spectra were taken.

with magnified vertical scales for the following time intervals: 0 to 2000 min, 2000 to 2500 min, and 4000 to 5000 s.

Consider the first 0 to 2000 min period, where the LIF laser was left at low intensity (100 W/cm^2) to minimize QD heating. As in Figure 3, the secular frequency undergoes a series of steps, with $\Delta\omega_z/e$ = 733.6 $\pm$ 5 Hz, averaged over the steps observed between 0 and 2000 min. Q was 17e at the onset and varied between 20 and 17 during this time period. The LIF intensity fluctuated in concert with the charge steps, due to the collection efficiency artifact discussed above. Just before 2000 min, the mass and LIF intensity measurements were interrupted to obtain spectral information by sequentially measuring LIF through a series of long-pass filters. During this interval, the mass and frequency series are not plotted and the LIF intensity is also perturbed by the filters. During this initial 2000 min low laser intensity period, the mass simply dropped slowly (1.07%/h), starting from an initial mass of 1877.8 $\pm$ 25.6 kDa, suggesting that this particle is an aggregate of either two or three QDs. Aggregates are probably present to some extent in the methanol-diluted electrospray solution used to get QDs into the gas phase, and additional aggregates may also form during electrospray. Such aggregate particles tend to have M/Q ratios greater than those for single QDs, and if desired, aggregates can largely be filtered out by operating the instrument at a trapping/guiding frequency of 280 kHz.[36]

At 2140 min, the LIF laser intensity was increased to ~216 W/cm^2 in order to heat the particle and then reduced back to 100 W/cm^2 (the original intensity) at 2380 min for another period of spectral measurements. As shown in Figures 4 and 5, the increase in laser power is accompanied by a sharp increase in emitted photon intensity and the beginning of a rapid decrease in the particle mass. The total mass loss during this first heating period was a factor of roughly two—too large to be explained entirely by ligand loss. In addition, a series

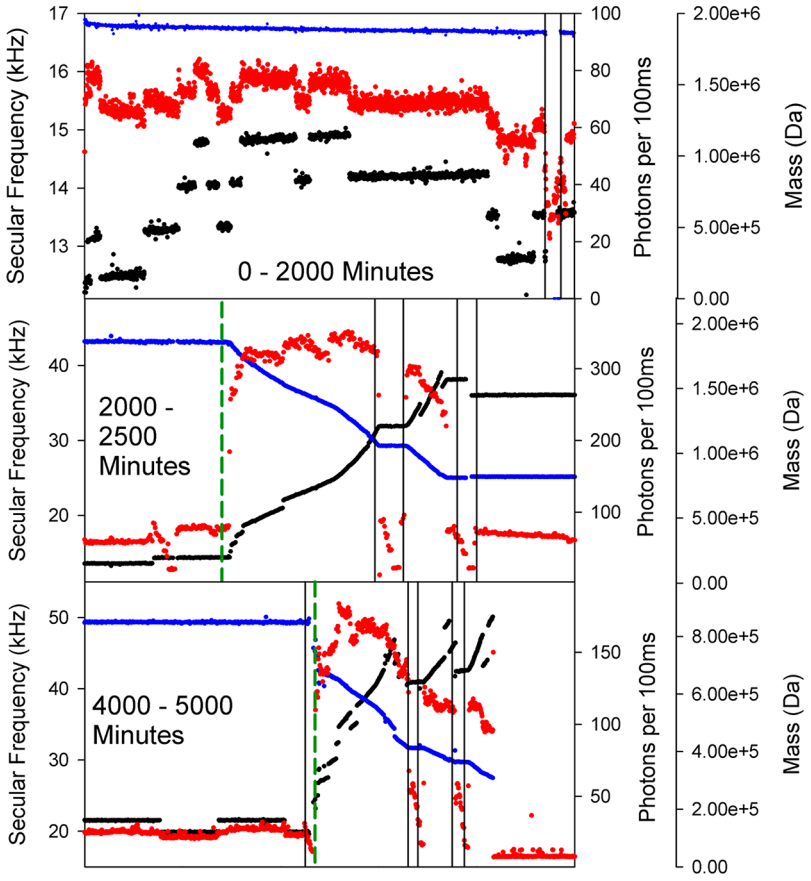

Figure 5. Detailed time records with expanded vertical scales for the particle in Figure 4 in the indicated time ranges.

of rapid charge steps, monotonically increasing the positive charge by 5*e*, were observed at the beginning of the heating period. Since the rate of collisions with electrons, Ar^+, and Ar* should not have increased dramatically (P_{trap} was not changed during the heating period), these rapid charge steps appear to indicate charging by thermionic electron emission. The fact that the rate of charging decreased with increasing particle charge is also consistent with this mechanism because electron binding energy should increase as the positive charge left behind increases, thus reducing the emission rate. Both the rapid mass loss and thermionic emission indicate that the temperature reached during this heating period was quite high, as discussed below. The electrons are clearly emitted from the surface layer, but the composition of this layer for a QD heated to such high temperatures is not clear. Due to diffusion, the surface may include atoms originally from the CdSe core, the ZnS shell, as well as carbonaceous material originating from the ligand layer.

The sharp increase in photon emission at higher LIF laser powers is expected, but given the observation of both sublimation and thermionic electron emission, it is likely that a substantial fraction of the increased photon emission is due to thermal ("black body") emission. It is for this reason that we turned the laser back to the initial intensity (100 W/cm^2) during the spectral measurement period between 2296 and 2325 min, so that the pre- and postheating spectra could be compared directly. In Figure 5, the effect of this interruption of the heating period is obvious. The mass and charge state both immediately stopped changing, and then mass loss resumed as soon as the laser intensity was increased back to 216 W/cm^2. Finally, at 2380 min, the heating period was terminated by reducing the laser intensity back to the original 100 W/cm^2 level, and the particle was monitored for 2000 min (~33 h).

During this "rest" period, the particle mass was nearly constant but initially *increased* by 3.3% during the first few hours, presumably due to adsorption of adventitious gases. The argon used as a buffer gas in these experiments was obtained from Airgas with stated impurities of H_2O (3 ppm) and O_2 (3 ppm), which would introduce ~10^{-9} Torr of both O_2 and H_2O, given the 1 mTorr Ar operating pressure. Furthermore, the base pressure in the chamber is in the 10^{-8} Torr range with H_2O being the main impurity, as determined with a residual gas analyzer, but also including smaller partial pressures of O_2, N_2, CO, CO_2, and hydrocarbons. The rate of mass gain over this time period (1.5 Da/s) is roughly consistent with these concentrations of adventitious adsorbates. For example, 1.5 Da/s corresponds to ~0.04 water molecules adding to the particle

per second, which would imply a water partial pressure of $\sim 10^{-7}$ Torr, with unit sticking probability. Given the presence of heavier reactants at lower partial pressures, the observed mass gain rate seems entirely reasonable.

At the beginning of the rest period, the charge state also showed signs of "recovering" from the high positive charge attained by thermionic emission at high temperature. A series of charge steps monotonically decreased the positive charge during the first few hours, as the highly positively charged particle preferentially combined with electrons. Only after the charge state had declined to $Q = 12-14$ did the charge begin to step bidirectionally, indicating that steady state had been reached. To probe the effects of these charge steps and surface reactions on the emission, spectra were acquired in two intervals, near the beginning and near the end of this rest period. Note that, during the rest period, the LIF intensity was only ~half that during the first 2000 min, presumably due to the reduction in particle mass. Nonetheless, it is interesting that the particle continued to be emissive even though it had such a large fraction of its mass during the heating period.

Finally, at $t = 4400$ min, the LIF laser intensity was again increased to 216 W/cm^2 and left high, allowing us to observe changes in mass, charge, and emission intensity as the particle sublimated. Note the rapid mass loss and the rapid charge stepping were interrupted by two brief periods where the laser intensity was reduced back to 100 W/cm^2 to allow spectral measurements. Emission was observed until, at 4836 min, the particle abruptly went dark. At that point, the mass was only 290 kDa, corresponding to loss of 84.7% of the initial particle mass, and the final observed charge was 13*e*. The simplest explanation for the final abrupt loss of emission would be ejection of the particle from the trap, and indeed, the final *M*/*Q* is outside the range recommended by Gerlich[1,37] for "safe" adiabatic trapping. As discussed below, however, there is actually still barely detectable emission after the "darkening" transition, leading us to conclude that the particle was still present.

Emission Spectrum. As noted, during several intervals over the course of the 83 h particle time record, emission spectral information was acquired using long-pass color filters on the APD detector. To avoid contributions to the signal from thermal emission, the LIF laser intensity was reduced to 100 W/cm^2 for each of these spectral measurement intervals. The data were converted to emission spectra by taking differences between intensities measured with successive filters, and the results are shown in Figure 6. Spectra are shown for each measurement interval indicated in Figure 4, along with an average of all the spectra. Because the total LIF intensity decreased as the particle sublimated, the spectra are normalized to allow easier comparison. In addition, the spectra are corrected for the APD sensitivity variations over the spectral range of interest, using quantum efficiency values provided for our APD module by the manufacturer. To test the filter/APD approach to spectral measurement, the spectrum for a solution of the QDs was measured using the same APD, color filters, and laser intensity, and this control spectrum is also shown. As expected from the manufacturer's data, the stock QD solution has an emission maximum at 550 nm, although we also see a small peak near 750 nm.

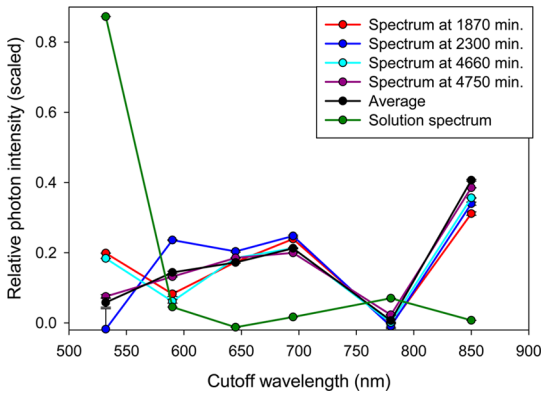

Figure 6. Emission spectra taken at the indicated times in Figures 4 and 5. An average of the spectra is shown, with error bars denoting the standard deviation of the four measurements. A solution-phase emission spectra was also obtained using the same optical arrangement for comparison (dashed line).

The emission spectra for the trapped gas-phase particle are significantly red-shifted with little intensity at 550 nm and most of the intensity in a broad peak between 590 and 695 nm. The emission also rises again toward 850 nm, suggesting that there may be a substantial peak in the near-IR. The possible origin of these spectral features is discussed below.

We have demonstrated that single QDs and small aggregates of QDs, isolated in the gas phase, have significant LIF quantum yields, and that the emission intensity is not strongly affected by changes in the charge. Furthermore, the QDs can be heated to temperatures where sublimation and thermal emission of electrons and photons is efficient yet still retain significant LIF quantum yield when the particles are allowed to cool again to temperature well below those required for significant thermal emission. Several points merit additional discussion.

DISCUSSION

Temperature Estimates for Heating and Rest Periods. As noted above, Figure 5 shows evidence that the QD aggregate reached temperatures during the "heating" periods high enough to drive sublimation and thermal emission. For reference, bulk ZnS is observed to sublime at about 1450 K,[38] although the temperature should be lower for small particles in vacuum. Bulk CdSe sublimes

at about 1420 K; however, sublimation of CdSe nanostructures in vacuum has been reported at temperatures as low as 773 K.[39]

Particle heating is *via* absorption of energy from the LIF laser, only part of which is radiated as fluorescence. A rough estimate of the heat deposition rate can be made using the LIF intensity to estimate the excitation rate. In Figure 3, and in the rest periods in Figure 4, where the particles show no signs of being hot enough for thermal emission or sublimation, it is reasonable to assume that the only significant emission process is LIF. Under these conditions, the LIF count rate was 500/s, and if we correct for APD quantum efficiency, reflection losses in the optics, and the collection solid angle, we can estimate that the particles were emitting on the order of 30 000 photons/s. A lower limit on the heating rate can be obtained by assuming that the LIF quantum yield is unity, so that the heating comes only from the Stokes shift between the 532 nm pump and the emission spectrum (Figure 6). Since we have no information on the spectral dependence of the emission at $\lambda \geq$ 850 nm, we assume that this near-IR emission is all at 900 nm for this estimation. With these assumptions, we reach a not unreasonable estimate for the heat deposition rate of ~16 000 eV/s ≈ 2.6 fW. If we assume that the heating rate for the higher laser power used in the heating periods in Figure 4 (for LIF count rate of 3300/s) is simply proportional to the increased laser power, the heat deposition rate would be ~105 000 eV/s ≈ 18 fW.

The particle temperature is set by the balance between these heat deposition rates and all cooling mechanisms. Since there is no evidence for thermal emission or rapid sublimation at the lower LIF laser intensity, the only significant cooling mechanism in that case is *via* collisions with the 1 mTorr of Ar buffer gas. The mean free path of the argon is much larger than the trap dimensions, and the velocities of the massive particles are negligible compared to the argon velocity. Therefore, the collisions are essentially of argon at the trap temperature (near 300 K) with the hot particle surface. The flux-weighted collisional cooling power can be estimated as

$$P = 2kAZ(T_{QD} - T_{trap}) \times \text{Accom}$$

where k is Boltzmann's constant, A is the surface area of the QD, Z is the collision rate per unit surface area, T_{QD} is the temperature of the QD, and Accom is an accommodation coefficient.[40] The accommodation coefficient accounts for the inelasticity of the Ar surface collisions, where Accom = 1 corresponds to collisions where the scattered argon is thermal at T_{QD} and Accom = 0 means no cooling. For a noble gas, Ar is a reasonably efficient collider, with, for example, Accom = 0.24 in collisions with a tungsten filament between 1073 and 1785 K.[41] For 1 mTorr of Ar at 300 K, there would be ~450 000 collisions per second with a single QD and roughly double that for a QD dimer, assuming that the QDs in the dimer remain unfused, which is probably a reasonable assumption for low temperatures. If we assume Accom = 0.24, then the collisional cooling power equals the laser heat deposition rate at T_{QD} = ~630 K. This is certainly (see below) well below the temperature where thermal electron or photon emission would be expected and thus seems reasonable. The slow mass losses seen in Figure 3 and the initial period in Figure 4 may indicate that sublimation is occurring, albeit very slowly, again, consistent with T_{QD} being below $T_{sublimation}$. Note that the measured mass losses of 1.0−1.1%/h correspond to a desorption rate of less than 5.8 Da/s.

If the higher heat load at high laser intensity was balanced only by collisional cooling, then the particle temperature would be ~2800 K; however, well below this temperature, additional cooling by sublimation and thermal emission of photons and electrons becomes significant. If the particles behaved like black bodies, the thermal photon emission would be governed by the Stefan−Boltzmann law:

$$P = A\epsilon\sigma T^4$$

where P is the radiated power, A is the surface area of the QD, ε is the emissivity constant, σ is Stefan's constant, and T is the temperature.[42] Subwavelength diameter particles do not behave as black bodies, however, and have emissivities well below unity and with substantial wavelength dependence.[43−45] A number of studies suggest that ϵ = 0.04 for refractory nanoparticles (W, Fe, and C).[46] For CdSe, ϵ = 0.001 might be a reasonable value since it is not a refractory material, and this should provide a reasonable lower bound on the radiative cooling. By itself, the thermal photon emission would balance the heating power at ~1300 K.

Thermionic emission of electrons is governed by the Richardson−Dushman equation: I(amps) = $AT^2 \exp(-\Phi/kT)$, where Φ is the material work function, and $A = 4\pi m_e e k^2/h^3$, where m_e and $-e$ are the electron mass and charge, k is the Boltzmann constant, and h is Planck's constant. The minimum energy carried away by each electron is Φ; however, because the electrons leave behind an increasingly positively charged particle, the actual energy loss per electron is significantly higher. Nonetheless, the frequency of electron emission is small—there are only 5 emission events between 2140 and 2210 min. Even taking the high positive charge (starting at 19e, rising to 24e) into account, the time-averaged cooling power from electron emission is only ~0.1 eV/s—negligible compared to the heating power.

Similarly, there is also a contribution to cooling from sublimation. During each high laser power heating period in Figure 4, the mass loss corresponds to ~40% of the initial particle mass; however, this corresponds to loss of only ~0.8 ZnS units/s or ~0.4 CdSe

units/s. The bulk heat of sublimation of CdSe and ZnS are, respectively, 405 kJ/mol (4.198 eV) and 468 kJ/mol (4.68 eV).[47] If we take the average of the two values, the sublimation cooling power is ~10 eV/s—large compared to that from thermionic emission, but still negligible compared to the laser heating power.

The particle temperature is set by the balance between laser heating power and the total cooling by collisions, sublimation, and thermal emission of electrons and photons; however, only collisions and thermal photon emission are significant. Taking both into account, the particle temperature is estimated to be ~1200 K; however, this estimate is certainly too high because, in estimating the laser heating rate, we assumed that all detected photons were LIF, whereas a significant fraction actually results from thermal emission. Correcting for this factor lowers the estimated temperature to ~1150 K. This should still be regarded as a crude estimate, due to uncertainties in the emissivity *versus* wavelength and other factors relating both to the laser heating and thermal emission cooling rates. Nonetheless, the estimated temperature is not unreasonable, in the sense that it is in the range where both sublimation and thermionic emission should be slow but observable. Because the rates for these processes are so strongly temperature-dependent, the temperature estimate is unlikely to be in error by more than ~100 K.

One other question is the extent to which thermal ("black body") photon emission contributes to the LIF signal seen under low power laser irradiation ($T_{QD} \approx$ 630 K). Figure 7 shows black body emission curves for 630 and 1150 K. It can be seen that the thermal contribution to the APD-sensitive wavelength range below 1000 nm is negligible at 630 K. The absence of thermal emission at the lower laser power was confirmed by measuring the effect of argon buffer gas pressure on the emission intensity, in the range from 1 to 30 mTorr. If thermal emission was significant, it would have been quenched at higher buffer gas pressure because T_{QD} is considerably lower (315 K from collisional cooling). No change in intensity was observed, ruling out a contribution from significant thermal emission at low laser power.

Nature of the Emission Process. The absorption and emission spectra for QDs in solution is dominated by exciton formation, as shown in Figure 6. This results in an emission band around 550 nm for the QDs used. However, the emission spectra acquired at various times for the trapped QD aggregate are significantly red-shifted with two peaks: one between 590 and 780 nm and the other above 850 nm. The differences between the gas-phase and solution-phase spectra cannot be attributed only to some effect of electrospray ionization because it has been shown that electrosprayed QDs deposited on surfaces have optical properties similar to those of the starting material.[48] Generally, red-shifted spectra, as seen in Figure 6, are a result of deep level emission from surface states, most commonly seen for small QDs where a majority of atoms are found on the surface or for high aspect ratio CdSe nanorods. In our case, the particle is likely an aggregate of 2 or 3 QDs, which possibly could coalesce into a single sphere when heated at high laser power. Coalescence would dramatically change the emission spectra in unknown ways because the core and the shell would mix, creating an ill-characterized nanoparticle. In this context, it is interesting that the emission spectra taken before and after periods of high power laser heating are not very different, even though there was mass loss and change in charge. This insensitivity to the details of the particle structure is consistent with emission from surface states, rather than core excitonic emission. The decrease in exciton emission must be

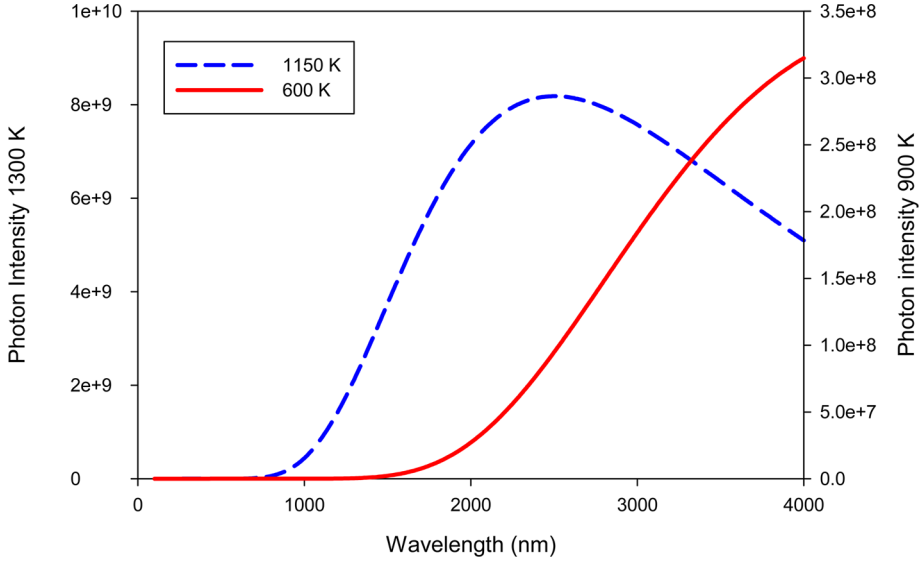

Figure 7. Black body emission curves for 1300 K (dashed blue line) and 600 K (solid red line).

due to an increased rate of the electron or hole diffusing to a surface state. Thus, surface states affect exciton emission by causing a decrease in the rate of radiative recombination of an electron and hole in the core of the QD.

Several other factors are consistent with the idea that we are observing emission from surface trap states. These tend to have a low quantum efficiency similar to our estimate of a ~0.2% quantum efficiency for the QD shown in Figure 5.[49,50] The quantum efficiency was calculated based on the absorption cross section determined by Leatherdale *et al.* and a particle size of 10 nm.[51] Considering the quantum efficiency is 0.2%, it is unlikely that multiexcitons are formed, but to confirm this, more studies are needed. Furthermore, if emission is from surface states, one might expect the intensity to scale with particle surface area. If the surface area is assumed to scale with the 2/3 power of the mass, then the emission intensity observed in the various low laser intensity periods is at least roughly consistent with the expected decrease in surface area with decreasing mass. For example, the emission intensity normalized to $M^{2/3}$ was 0.046 prior to heating and 0.035 for the postheated particle which had lost substantial mass. Given that we have no information about the shape of the aggregate particle and how it evolves with heating, the agreement with surface area scaling is reasonable, though certainly not definitive. The difference in the solution spectrum and the spectra of a single QD, shown in Figure 6, indicates that the surface states are not intrinsic to the QDs used in this study but are, rather, created in the trapped particles by some combination of charging, heating, and ligand loss. A factor to consider is that there is a ~12% lattice mismatch between CdSe and ZnS in the bulk.[52,53] Thus interdiffusion/mixing of the core and shell upon heating would tend to create additional defects at the core−shell interface.

Heating to "Darkness". Figure 5 shows the final time period, where the particle is heated until it finally goes "dark". The total mass at that point is about what we would expect for a single CdSe core (290 kDa). Emission spectra were acquired in several intervals during the final heating period, and for these, the laser intensity was returned to the same low (100 W/cm^2) level used for all the other emission spectra, where thermal emission makes a negligible contribution (see above). As shown in Figure 6, the emission spectra taken late in the sublimation process are not radically different from those taken before significant mass loss occurred, although the intensity is significantly lower, even before the final abrupt "darkening" transition at 4836 min. This slow decrease in emission intensity may simply reflect a decrease in surface area of the particle, particularly if surface states are involved in the observed red-shifted emission. Note that there is also a slow decrease in fluorescence intensity at high laser intensity, where thermal emission is expected to make a significant contribution and surface area certainly plays a role in this case.

One question is whether the final abrupt near-total loss of emission at 4836 min results from the particle no longer absorbing the 532 nm laser, or if the particle continues to absorb, but with near-zero fluorescence quantum yield. If the latter explanation were true, we would still expect to see thermal emission from the hot particle—indeed, the temperature should increase if the absorbed laser energy is no longer partly radiated as fluorescence. Therefore, we tentatively conclude that the loss of emission reflects a sudden loss of absorption, which is not unexpected. The band gap for the QD should increase with decreasing size, and at some point, the 532 nm laser would simply no longer be able to excite the particle. Because we are not averaging over a distribution of QDs, the drop in excitation rate could be abrupt. Note that, as soon as the particle stops absorbing, its temperature would rapidly drop to ~300 K.

Blinking after Darkening of the Particle. During the ~80 h preceding the final darkening transition at 4836 min, the particle in Figures 4 and 5 was never observed to blink (*i.e.*, show intermittent fluorescence). However, after the final darkening transition, the small remaining signal shows significant intermittency if it is binned in 1 or 10 s time intervals. Figure 8 shows a 14 h continuation of the signal record, starting just after the abrupt darkening transition, binned in 1 s intervals. Figure 9 shows a histogram of the intensity levels observed and the distributions of bright ("on") and dark ("off") time intervals. The intensity histogram is clearly bimodal, with the major peak simply reflecting the APD dark count rate, but with a small peak at about twice the dark count level. The on/off distributions show that there are reasonably frequent "on" intervals lasting between 1 and 20 s, but that the "off" intervals are much longer, consistent with the histogram showing that the particle is dark most of the time.

It is not clear why this particle, having lost ~85% of its initial mass and having apparently ceased to absorb the 532 nm pump laser, should show intermittent emission. One possibility is that, in the nonabsorbing state, with T_{QD} = 300 K, the particle slowly absorbs or reacts with background gases, modifying the surface such that the band gap becomes small enough to allow 532 nm absorption again. At that point, the particle would heat rapidly, presumably driving off the adsorbed surface species within seconds, increasing the band gap, and causing the particle to stop absorbing again. In this scenario, the "on" times should be short because surface species should desorb rapidly from the particle once it begins to absorb again. The "off" times should be much longer, determined by the time it takes for adsorption of appropriate adventitious species from the chamber background. As discussed

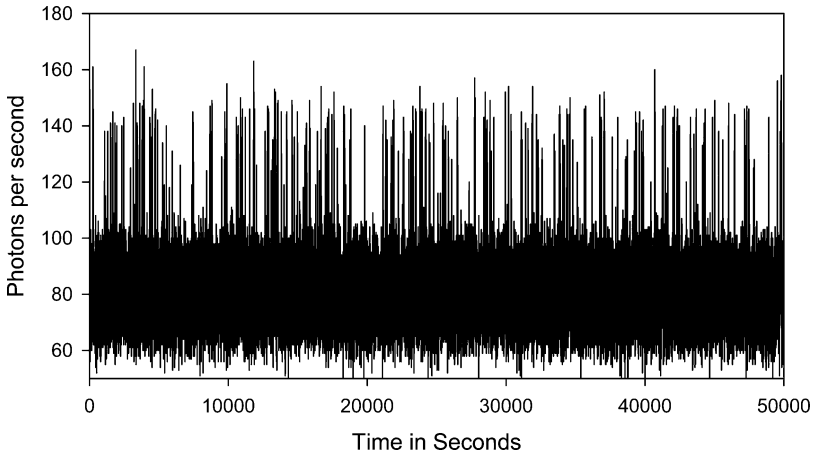

Figure 8. Time record for the first 50 000 s after the QD from Figures 4 and 5 went "dark".

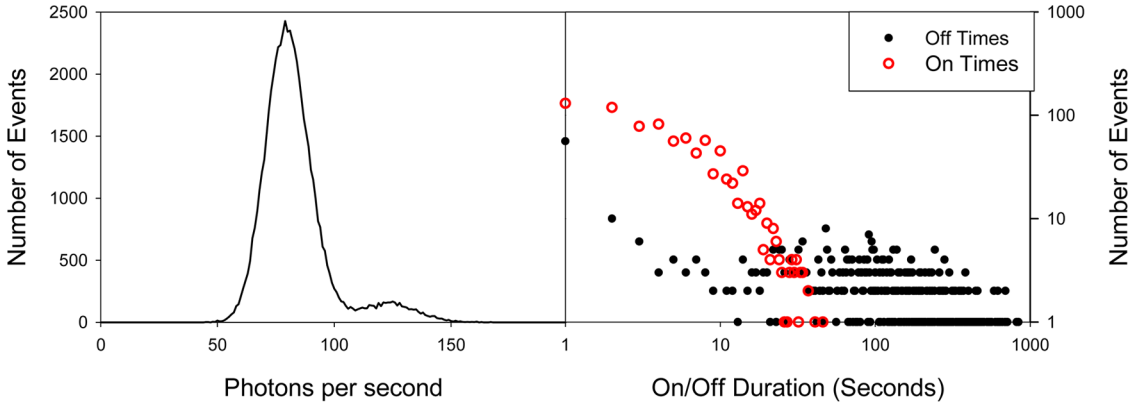

Figure 9. Left: Histogram of brightness levels observed in Figure 8. Right: Duration distributions of "on" (open red circles) and "off" times (black filled circles) in the time record in Figure 8. The on/off cutoff was chosen as 107 photons per second.

above, species such as water, oxygen, CO, CO_2, and hydrocarbons are present at concentrations that lead to slow mass gain. Such a scenario could go on indefinitely, and as shown in Figure 8, rather stable blinking behavior was still occurring after almost 14 h of monitoring.

CONCLUSIONS

In conclusion, we have demonstrated that it is possible to trap single QDs and small QD aggregates in a split-ring quadrupole trap and report the fluorescence and thermal emission behavior of QDs in the gas phase. It is possible to detect strong fluorescence from a single QD, after brightening the QD by brief CO_2 laser heating of the ligand layer. The mass and charge of trapped particles are easily determined by secular frequency measurements and can be tracked for long times as the particles are manipulated by heating and exposure to charge changing collisions. Obviously, other manipulations, such as exposure to reactive gases to carry out surface chemical modification, are possible. The emission spectra of a single QD aggregate showed a significant red shift that would be expected from solution-phase measurements. More studies are needed to understand the mechanism of fluorescence, the QD going dark, and blinking. We are confident that NPMS is a suitable and powerful tool to uncover these mechanisms.

METHODS

The instrument, described elsewhere,[36] consists of an electrospray source used to get nanoparticles into the gas phase, a hexapole guide for differential pumping and desolvation, a quadrupole ion guide used to prefilter the *M*/*Q* distribution fed to the trap, and finally the split-ring electrode quadrupole trap (SRET), which was based on a design by Gerlich and co-workers,[54] as shown in Figure 1. Water-soluble core−shell CdSe/ZnS (with mercaptoundecanoic acid as a ligand) QDs were obtained from NN-Labs. The QDs used in these studies have a solution-phase emission maximum near 550 nm, although it is not obvious what to expect for charged QDs in the gas phase. The QD stock solution was diluted in methanol (1:100) and electrosprayed in a Micromass (now Waters) z-spray source with a capillary voltage of 3.5 kV and a cone voltage of 210 V. Positive ions formed by the electrospray source were guided through the hexapole ion guide

at a pressure of ~20 mTorr to collisionally cool and focus the particle beam. We presume that the presence of positive ions in the solution (mostly Na^+) was responsible for the initial charging of the QDs. The QDs passed from the hexapole, through a pneumatically operated isolation valve, and into a linear quadrupole guide, which has similar trapping properties to those of the SRET, and therefore functions as a prefilter to reject ions and particles outside the *M/Q* range of interest. From the linear quadrupole guide, the QDs are injected into the trap using 15 mTorr of argon buffer gas to aid trapping and damp the initial kinetic energy of the trapped QD. With the isolation valve closed, the base pressure in the trap chamber is $\sim 2 \times 10^{-8}$ Torr. While trapping, both the 532 nm laser (100 W/cm^2) and the CO_2 laser (1000 W/cm^2) were focused through the trap to enable immediate detection of the trapped QD. To inject a QD, the isolation valve was repeated pulsed open (open time ~1 s), while monitoring LIF signal, looking for the signature of a trapped QD (~300−500 counts per second). TTL pulses from the APD were counted by a ComTec multichannel scalar (P7882). As soon as signal was observed, the CO_2 laser was turned off, and the pressure was dropped to between 0.1 and 1 mTorr, and a scan of ω_z was made to verify that only a single particle was trapped (80% of the time). In the event that more than one secular frequency resonance was observed, the trap was simply dumped and the fill process was restarted.

Ion Trap and Optical Detection. The SRET is a type of Paul trap, with the center ring electrode split to allow optical access through the trap. In addition, the end-cap electrodes are truncated cones with holes to allow a particle beam to pass through along the trap axis. We added a pair of diagonal channels that allow lasers to be focused through the trap center, and for the work presented here, one pair was used, together with a pair of confocal off-axis paraboloidal mirrors, to focus a CO_2 laser (Synrad, 10 W, duty cycle modulated) through the trap for particle heating. Near the electrodes, the fields are far from the fields in an ideal hyperbolic Paul trap; however, for sufficiently small excursions from the trap center, the nonidealities are small. Under appropriate operating conditions,[10,16,55] the motion in such a trap is harmonic, with well-defined frequencies associated with radial and axial motion, ω_r and ω_z, respectively. Either of the frequencies can be used to calculate the *M/Q* ratio for the trapped particle, but in our geometry, ω_z is more easily and precisely measured, and in this case, $M/Q = (\sqrt{2}V_0)/(\omega_z \Omega z_0^2)$, where V_0 and Ω are the amplitude and frequency of the radio frequency voltage applied to the trap ($V_0 = 500$ V, $\Omega/2\pi = 143.3$ kHz), and z_0 (2.96 mm) is a parameter describing the field geometry.

Particles were detected by focusing a cw 532 nm laser (Ultra Lasers) through the trap (into the page on Figure 1) with a beam waist diameter of ~100 μm to excite fluorescence of the trapped QD. The effects of varying the laser intensity between roughly 100 and 220 W/cm^2 are also examined. Fluorescence emitted from the QDs in the trap was collimated by an aspheric lens with a 25 mm focal length, passed through a 532 nm notch filter to block scattered light, and focused onto an avalanche photodiode module (APD) (Laser Components: Count). To obtain emission spectral information, long-pass filters with cutoff wavelengths of 590, 645, 695, 780, and 850 nm (Thorlabs) were installed in line with the APD.

We operated the CO_2 laser at a 50% duty cycle (5 W average power) during particle injection because we find that this leads to substantial increase in fluorescence quantum yield, making the particles much easier to detect. The mechanism of this "brightening" process is not completely understood; however, the mercaptoundecenoic acid ligand layer has an absorption band at 10.6 μm and therefore should be heated by the CO_2 laser, while neither CdSe and ZnS absorb strongly at 10.6 μm (absorption coefficient 0.016[56] and 0.2 cm^{-1},[57] respectively). Therefore, it appears that the brightening process involves heating the ligand layer, possibly driving additional loss of solvent molecules or some ligand desorption. Additional studies of this phenomenon are planned.

Safety. Since cadmium is toxic, precautions were taken to avoid contact with the particles. The electrospray source is contained within a glass cylinder to ensure that CdSe/ZnS particles do not spray into the atmosphere. The glass cylinder and other electrospray components were periodically cleaned in methanol. Whenever handling particles or contaminated parts, it is important to wear necessary attire (gloves, eye protection). Syringes and used solvent are hazardous waste and must be disposed of appropriately.

Conflict of Interest: The authors declare no competing financial interest.

Acknowledgment. We would like to thank D. Gerlich of Technical University Chemnitz, M. Bartl and J. Gerton of the University of Utah, and J. Hollingsworth of Los Alamos National Laboratories for helpful discussions. The work was supported by the Chemistry Division of the U.S. National Science Foundation, under Grant CHE-1111935.

REFERENCES AND NOTES

1. Schlemmer, S.; Illemann, J.; Wellert, S.; Gerlich, D. Nondestructive High-Resolution and Absolute Mass Determination of Single Charged Particles in a Three-Dimensional Quadrupole Trap. *J. Appl. Phys.* **2001**, *90*, 5410–5418.
2. Grimm, M.; Langer, B.; Schlemmer, S.; Lischke, T.; Widdra, W.; Gerlich, D.; Becker, U.; Ruehl, E. New Setup To Study Trapped Nano-particles Using Synchrotron Radiation. *AIP Conf. Proc.* **2004**, *705*, 1062–1066.
3. Schlemmer, S.; Wellert, S.; Windisch, F.; Grimm, M.; Barth, S.; Gerlich, D. Interaction of Electrons and Molecules with a Single Trapped Nanoparticle. *Appl. Phys. A: Mater. Sci. Process* **2004**, *78*, 629–636.
4. Grimm, M.; Langer, B.; Schlemmer, S.; Lischke, T.; Becker, U.; Widdra, W.; Gerlich, D.; Flesch, R.; Ruehl, E. Charging Mechanisms of Trapped Element-Selectively Excited Nanoparticles Exposed to Soft X-rays. *Phys. Rev. Lett.* **2006**, *96*, 066801/1–066801/4.
5. Davis, E. J.; Ray, A. K. Single Aerosol Particle Size and Mass Measurements Using an Electrodynamic Balance. *J. Colloid Interface Sci.* **1980**, *75*, 566–576.
6. Kane, B. E. Levitated Spinning Graphene Flakes in an Electric Quadrupole Ion Trap. *Phys. Rev. B* **2010**, *82*, 115441–115454.
7. Yin, Z.-q.; Li, T.; Zhang, X.; Duan, L. M. Large Quantum Superpositions of a Levitated Nanodiamond through Spin-Optomechanical Coupling. *Phys. Rev. A* **2013**, *88*, 33614–33620.
8. Gieseler, J.; Deutsch, B.; Quidant, R.; Novotny, L. Subkelvin Parametric Feedback Cooling of a Laser-Trapped Nanoparticle. *Phys. Rev. Lett.* **2012**, *109*, 103603–103608.
9. Bell, D. M.; Howder, C. R.; Gerlich, D.; Lewis, D. K.; Anderson, S. L. Non-destructive, High Precision Mass Determination for Single, Trapped, Gigadalton Nanoparticles. Manuscript in preparation.
10. Schlemmer, S.; Illemann, J.; Wellert, S.; Gerlich, D. Nondestructive, Absolute Mass Determination of Sub-Micrometer Sized Particles in a Paul-Type Trap. *AIP Conf. Proc.* **1999**, *457*, 80–84.
11. Trevitt, A. J.; Wearne, P. J.; Bieske, E. J. Calibration of a Quadrupole Ion Trap for Particle Mass Spectrometry. *Int. J. Mass Spectrom.* **2007**, *262*, 241–246.
12. Cai, Y.; Peng, W. P.; Kuo, S. J.; Lee, Y. T.; Chang, H. C. Single-Particle Mass Spectrometry of Polystyrene Microspheres and Diamond Nanocrystals. *Anal. Chem.* **2002**, *74*, 232–238.
13. Cai, Y.; Peng, W. P.; Kuo, S. J.; Sabu, S.; Han, C. C.; Chang, H. C. Optical Detection and Charge-State Analysis of MALDI-Generated Particles with Molecular Masses Larger than 5 MDa. *Anal. Chem.* **2002**, *74*, 4434–4440.
14. Peng, W. P.; Cai, Y.; Lee, Y. T.; Chang, H. C. Laser-Induced Fluorescence/Ion Trap as a Detector for Mass Spectrometric Analysis of Nanoparticles. *Int. J. Mass Spectrom.* **2003**, *229*, 67–76.
15. Peng, W.-P.; Yang, Y.-C.; Kang, M.-W.; Lee, Y. T.; Chang, H.-C. Measuring Masses of Single Bacterial Whole Cells with a Quadrupole Ion Trap. *J. Am. Chem. Soc.* **2004**, *126*, 11766–11767.

16. Dawson, P. H. *Quadrupole Mass Spectrometry*; Elsevier Scientific: Amsterdam, 1976; pp 1−349.
17. Wuister, S. F.; Swart, I.; van Driel, F.; Hickey, S. G.; Donegá, C. D. M. Highly Luminescent Water-Soluble CdTe Quantum Dots. *Nano Lett.* **2003**, *3*, 503–507.
18. Donegá, C. D. M.; Hickey, S. G.; Wuister, S. F.; Vanmaeckelbergh, D.; Meijerink, A. Single-Step Synthesis To Control the Photoluminescence Quantum Yield and Size Dispersion of CdSe Nanocrystals,. *J. Phys. Chem. B* **2003**, *107*, 489–496.
19. Shim, M.; Wang, C.; Sionnest, P. G. Charge-Tunable Optical Properties in Colloidal Semiconductor Nanocrystals. *J. Phys. Chem. B* **2001**, *105*, 2369–2373.
20. Wang, C.; Wehrenberg, B. L.; Woo, C. Y.; Guyot-Sionnest, P. Light Emission and Amplification in Charged CdSe Quantum Dots. *J. Phys. Chem. B* **2004**, *108*, 9027–9031.
21. Guyot-Sionnest, P. Charging Colloidal Quantum Dots by Electrochemistry. *Microchim. Acta* **2008**, *160*, 309–314.
22. Jha, P. P.; Guyot-Sionnest, P. Electrochemical Switching of the Photoluminescence of Single Quantum Dots. *J. Phys. Chem. C* **2010**, *114*, 21138–21141.
23. Qin, W.; Shah, R. A.; Guyot-Sionnest, P. CdSeS/ZnS Alloyed Nanocrystal Lifetime and Blinking Studies under Electrochemical Control. *ACS Nano* **2012**, *6*, 912–918.
24. Galland, C.; Ghosh, T.; Steinbruck, A.; Sykora, M.; Hollingsworth, J. A.; Klimov, V. I.; Htoon, H. Two Types of Luminescence Blinking Revealed by Spectroelectrochemistry of Single Quantum Dots. *Nature* **2011**, *479*, 203–207.
25. Ding, Z.; Quinn, B. M.; Haram, S. K.; Pell, L. E.; Korgel, B. A.; Bard, A. J. Electrochemistry and Electrogenerated Chemiluminescence from Silicon Nanocrystal Quantum Dots. *Science* **2002**, *296*, 1293–1297.
26. Myung, N.; Ding, Z.; Bard, A. J. Electrogenerated Chemiluminescence of CdSe Nanocrystals. *Nano Lett.* **2002**, *2*, 1315–1319.
27. Lesnyak, V.; Gaponik, N.; Eychmuller, A. Colloidal Semiconductor Nanocrystals: The Aqueous Approach. *Chem. Soc. Rev.* **2013**, *42*, 2905–2929.
28. Kim, J. Y.; Voznyy, O.; Zhitomirsky, D.; Sargent, E. H. 25th Anniversary Article: Colloidal Quantum Dot Materials and Devices: A Quarter-Century of Advances. *Adv. Mater.* **2013**, *25*, 4986–5010.
29. Brichkin, S. B.; Chernykh, E. V. Hydrophilic Semiconductor Quantum Dots. *High Energy Chem.* **2011**, *45*, 1–12.
30. Kongkanand, A.; Tvrdy, K.; Takechi, K.; Kuno, M.; Kamat, P. V. Quantum Dot Solar Cells. Tuning Photoresponse through Size and Shape Control of CdSe−TiO_2 Architecture. *J. Am. Chem. Soc.* **2008**, *130*, 4007–4015.
31. Turdy, K.; Frantsuzov, P. A.; Kamat, P. V. Photoinduced Electron Transfer from Semiconductor Quantum Dots to Metal Oxide Nanoparticles. *Proc. Natl. Acad. Sci. U.S.A.* **2011**, *108*, 29–34.
32. Sargent, E. H. Colloidal Quantum Dot Solar Cells. *Nat. Photonics* **2012**, *6*, 133–135.
33. Xiong, W.; Hickstein, D. D.; Schnitzenbaumer, K. J.; Ellis, J. L.; Palm, B. B.; Keister, K. E.; Ding, C.; Miaja-Avila, L.; Dukovic, G.; Jimenez, H. C. Photoelectron Spectroscopy of CdSe Nanocrystals in the Gas Phase: A Direct Measure of the Evanescent Electron Wave Function of Quantum Dots. *Nano Lett.* **2013**, *13*, 2924–2930.
34. Decker, S. Untersuchung von Fullerenen im Strahlungsgleichgewicht. *Wiss. Z. Tech. Univ. Chemnitz* **2010**.
35. Zhang, Y.; Schnoes, A. M.; Clapp, A. R. Dithiocarbamates as Capping Ligands for Water-Soluble Quantum Dots. *ACS Appl. Mater. Interfaces* **2010**, *2*, 3384–3395.
36. Howder, C. R.; Bell, D. M.; Anderson, S. L. Optically Detected, Single Nanoparticle Mass Spectrometer with Prefiltered Electrospray Nanoparticle Source. *Rev. Sci. Instrum.* **2013**, DOI: dx.doi.org/10.1063/1.4861923.
37. Gerlich, D. Molecular Ions and Nanoparticles in RF and AC Traps. *Hyperfine Interact.* **2003**, *146/147*, 293–306.
38. Zinc Sulfide. http://www.inchem.org/documents/icsc/icsc/eics1627.htm, *IPCS International Programme on Chemical Safety*, Ed. 2005.
39. Goris, B.; Van Huis, M. A.; Bals, S.; Zandbergen, H. W.; Manna, L.; Van Tendeloo, G. Thermally Induced Structural and Morphological Changes of CdSe/CdS Octapods. *Small* **2012**, *8*, 937–942.
40. Hansen, K. *Statistical Physics of Nanoparticles in the Gas Phase*; Spring Science+Buisness Media: Dordrecht, The Netherlands, 2013; Vol. 73.
41. Watt, W.; Moreton, R.; Carpenter, L. G. The Thermal Accommodation of Helium and Argon on a Tungsten Wire, Deduced from the Heat Lost by the Wire. *Surf. Sci.* **1974**, *45*, 238–248.
42. Roura, P.; Costa, J. Radiative Thermal Emission from Silicon Nanoparticles: A Reversed Story from Quantum to Classical Theory. *Eur. J. Phys.* **2002**, *23*, 191–203.
43. Landstrom, L.; Elihn, K.; Boman, M.; Granqvist, C. G.; Heszler, P. Analysis of Thermal Radiation from Laser-Heated Nanoparticles Formed by Laser-Induced Decomposition of Ferrocene. *Appl. Phys. A: Mater. Sci. Process.* **2005**, *81*, 827–833.
44. Yu, S.-J.; Youn, S. J.; Kim, H. Size Effect of Thermal Radiation. *Physica B* **2010**, *405*, 638–641.
45. Odashima, H.; Tachikawa, M.; Takehiro, K. Mode-Selective Thermal Radiation from a Microparticle. *Phys. Rev. A* **2009**, *80*, 41806–41810.
46. *Gas Phase Nanoparticle Synthesis*; Kluwer Academic Publishers: Dordrecht, The Netherlands, 2004.
47. Szentpaly, L. V. Atom-Based Thermochemistry: Predictions of the Sublimation Enthalpies of Group 12 Chalcogenides and the Formation Enthalpies of their Polonides. *J. Phys. Chem. A* **2008**, *112*, 12695–12701.
48. Pease, L. F., III; Feldblyum, J. I.; Lacaerda, S. H. D.; Liu, Y.; Walker, A. R. H.; Anumolu, R.; Yim, P. B.; Clarke, M. L.; Kang, H. G.; Hwang, J. Structural Analysis of Soft Multicomponent Nanoparticle Clusters. *ACS Nano* **2010**, *4*, 6982–6988.
49. Kim, J. I.; Kim, J.; Lee, J.; Jung, D.-R.; Kim, H.; Choi, H.; Lee, S.; Byun, S.; Kang, S.; Park, B. Photoluminescence Enhancement in CdS Quantum Dots by Thermal Annealing. *Nanoscale Res. Lett.* **2012**, *7*, 482–489.
50. Saunders, A. R.; Ghezelbash, A.; Sood, P.; Korgel, B. A. Synthesis of High Aspect Ratio Quantum-Size CdS Nanorods and Their Surface-Dependent Photoluminescence. *Langmuir* **2008**, *24*, 9043–9049.
51. Leatherdale, C. A.; Woo, W.-K.; Mikulec, F. V.; Bawendi, M. G. On the Absorption Cross Section of CdSe Nanocrystal Quantum Dots. *J. Phys. Chem. B* **2002**, *106*, 7619–7622.
52. Dabbousi, B. O.; Rodriguez-Viejo, J.; Mikulec, F. V.; Heine, J. R.; Mattoussi, H.; Ober, R.; Jensen, K. F.; Bawendi, M. G. (CdSe)ZnS Core−Shell Quantum Dots: Synthesis and Characterization of a Size Series of Highly Luminescent Nanocrystallites. *J. Phys. Chem. B* **1997**, *101*, 9463–9475.
53. Smith, A. M.; Nie, S. Semiconductor Nanocrystals: Structure, Properties, and Band Gap Engineering. *Acc. Chem. Res.* **2010**, *43*, 190–200.
54. Gerlich, D.; Decker, S. Trapping Ions at High Temperatures: Thermal Decay of C_{60}^+. *Appl. Phys. B* **2013**, DOI: 10.1007/s00340-013-5668-y.
55. Gerlich, D. Inhomogeneous Electrical Radio Frequency Fields: A Versatile Tool for the Study of Processes with Slow Ions. In *Advances in Chemical Physics: State-Selected and State-To-State Ion−Molecule Reaction Dynamics, Part 1*; Ng, C. Y., Baer, M., Eds.; John Wiley & Sons: New York, 1992; Vol. 82, pp 1−176.
56. Cadmium Selenide (CdSe) Absorption, Reflection, Luminescence. In *II-VI and I-VII Compounds; Semimagnetic Compounds*, Madelung, O., Rössler, U., Schulz, M., Eds.; Springer: Berlin: 1999; Vol. 41B, pp 1−7.
57. Zinc Sulfide−ZnS and ZnS Clear. http://www.schott.com/advanced_optics/english/download/schott_zinc_sulfide_may_2011_eng.pdf, 2013.